Nanoelectronics and Its New Materials – A NEW ERA OF NANOSCIENCE

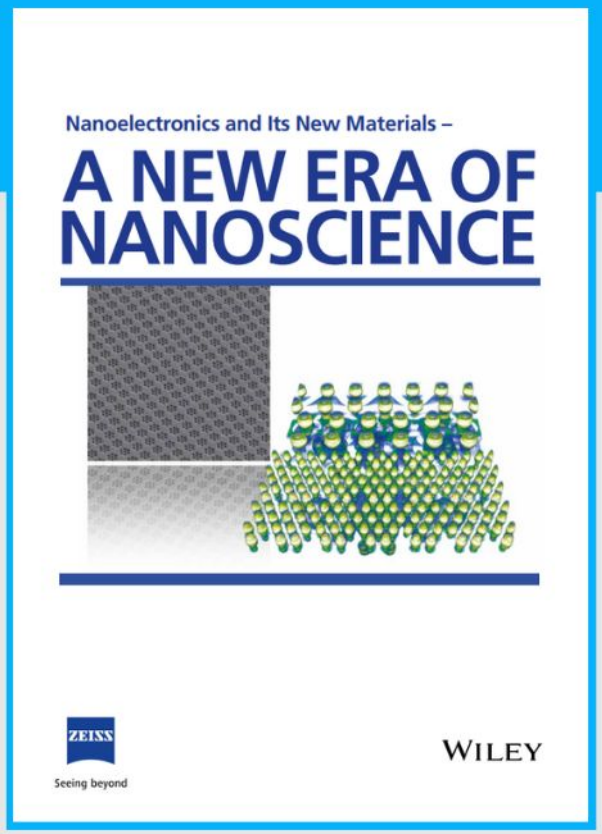

Discover the recent advances in electronics research and fundamental nanoscience.

Nanotechnology has become the driving force behind breakthroughs in engineering, materials science, physics, chemistry, and biological sciences. In this compendium, we delve into a wide range of novel applications that highlight recent advances in electronics research and fundamental nanoscience. From surface analysis and defect detection to tailored optical functionality and transparent nanowire electrodes, this eBook covers key topics that will revolutionize the future of electronics.

To get your hands on this valuable resource and unleash the power of nanotechnology, simply download the eBook now. Stay ahead of the curve and embrace the future of electronics with nanoscience as your guide.

ZEISS

Seeing beyond

WILEY

NANO · MICRO small
www.small-journal.com

Salt-Adaptively Conductive Ionogel Sensor for Marine Sensing

Huijing Li, Long Li, Junjie Wei, Tao Chen,* and Peng Wei**

Hydrophobic ionogel has attracted much attention in underwater sensing as the artificial electronic skins and wearable sensors. However, when the low conductive ionogel-based sensor works in the marine environment, the salty seawater weakens its sensing performance, which is difficult to recognize. Herein, a salt-adaptively conductive ionogel with high submarine strain sensitivity is reported. Based on the preliminary improvement via the proton conduction mechanism, the conductivity of the ionogel further increases with the surrounding salinity rising up since the salt-induced dissociation phenomenon, which is described as the environmental salt-adaptive feature. In seawater, the conductivity of the ionogel is as high as 2.90×10^{-1} S m^{-1}. Significantly, with its long-term underwater stability and adhesion, the resultant ionogel-based sensor features prominent strain sensing performance (gauge factor: 1.12) while combining with various soft actuators in the marine environment. The ionogel-based sensor is capable of monitoring human breath frequency, human actions, and the locomotion of soft actuators, demonstrating its great potential in diving detection and intelligent preceptive soft robotics for marine environmental protection and exploration.

1. Introduction

The ocean, one of Earth's most diverse ecosystems areas, is fully attractive for scientists to explore. However, unlike working and living in atmospheric conditions, robotics and humanity in marine have to face significantly different parameters, for instance, humidity, pressure, visibility, and environmental conductivity.[1] As a result, monitoring and controlling humanity and robotics in this challenging environment is essential for their safety. For this, although various soft wearable electronics based on soft materials,[2] especially gel-based sensors, have attracted considerable attention with their merits of softness and stretchability, their underwater application is usually susceptible.[3] For example, the hydrophilic nature of gel-based sensors causes underwater swelling and ionic diffusion drawbacks, negatively impacting long-term stable working in the aquatic environment.[4] To overcome the above-mentioned shortcomings, a great deal of effort has been dedicated to improving the water resistance of gel-based materials.[5] For example, Qu and co-workers reported an ionic skin which can keep stable in various environments,[6] including underwater, by isolating the conductive gel from surroundings with two protective layers covering. This packaging method with the additional waterproof film is one of the simplest ways to prevent direct contact of gel with environmental water, nevertheless, the mechanical properties of the resultant sensor are restricted by that of the cover film rather than the gel.[6,7] To abandon the packaging materials, the conductive gel can be featured with hydrophobic nature. Ionogel-based sensors with hydrophobic conductive ionic liquid (IL) attract tremendous attention in recent years.[8] Yu and Wu fabricated an ionogel by polymerization of fluorine-rich ionic liquid monomers in another fluorine-rich ionic liquid.[9] Owing to the low surface energy and moisture absorption features of fluoropolymers, the ionogel eliminated the interference from water molecules, realizing long-term structural and component stability in the aquatic environment.

However, different from the experimental pure water environment, nature waters (e.g., salt lakes and oceans) are always saline solutions, which would interfere with the electrical sensing performance of the naked ionogel with their conductivity. In other words, when it is sensing in saline water, the naked ionogels could be regarded as parallel connected with the environmental resistor in the sensing circuitry. Due to the relatively low conductivity of the ionogel, the sensing signal (resistance change) is gradually weakened and dominated by the environmental solution conductivity. For example, in the work of Chen and co-workers,[10] with higher surrounding salinity, the detection signal becomes weaker and more difficult to distinguish. To improve

H. Li, L. Li, J. Wei, T. Chen
Key Laboratory of Marine Materials and Related Technologies
Zhejiang Key Laboratory of Marine Materials and Protective Technologies
Ningbo Institute of Material Technology and Engineering
Chinese Academy of Sciences
Ningbo 315201, China
E-mail: weijunjie@nimte.ac.cn; tao.chen@nimte.ac.cn
H. Li, L. Li, J. Wei, T. Chen
School of Chemical Science
University of Chinese Academy of Sciences
19A Yuquan Road, Beijing 100049, China
P. Wei
Department of Plastic and Reconstructive Surgery
Ningbo First Hospital
Ningbo 315010, China
E-mail: weipeng@nbu.edu.cn

The ORCID identification number(s) for the author(s) of this article can be found under https://doi.org/10.1002/smll.202305848

DOI: 10.1002/smll.202305848

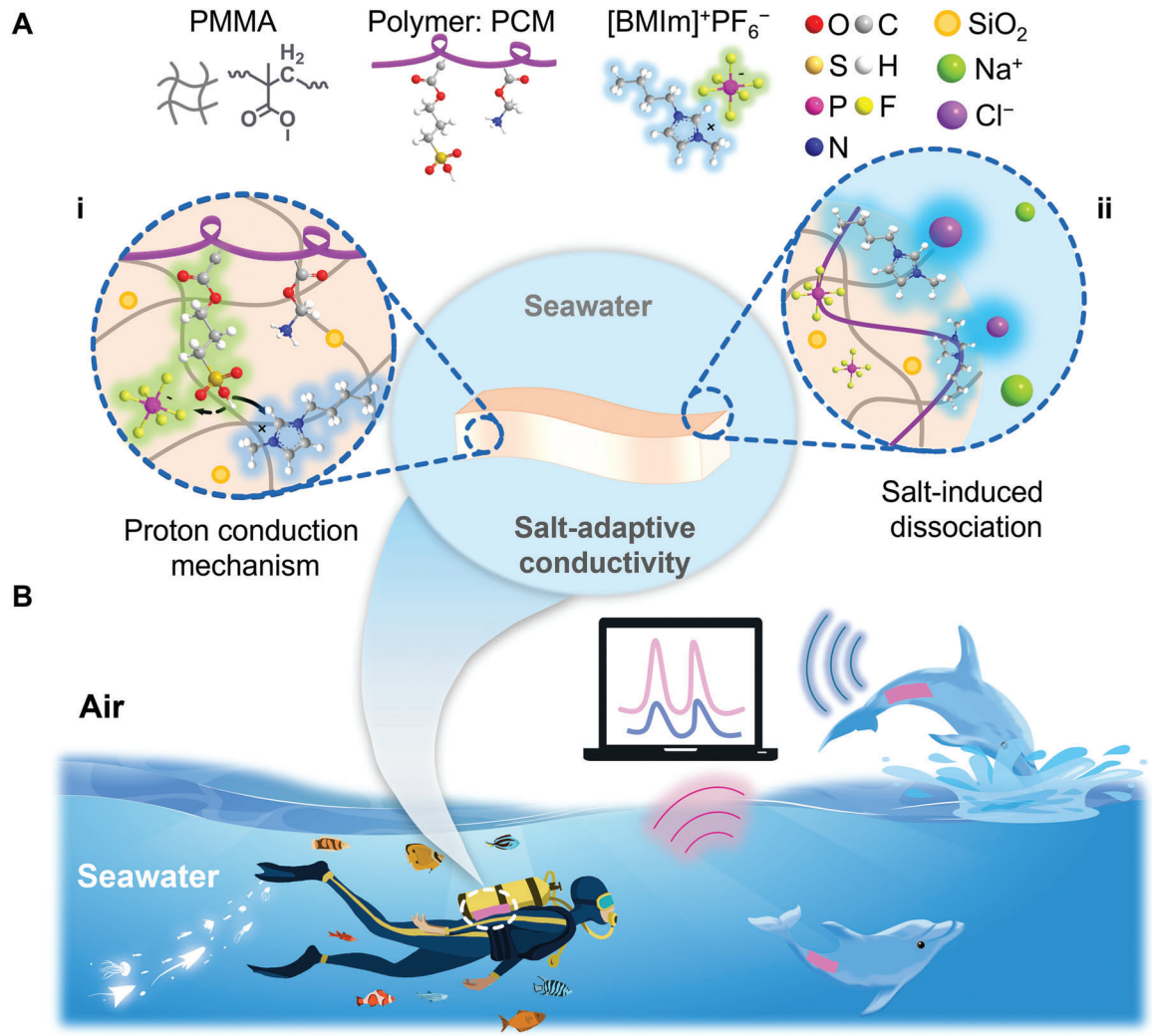

Figure 1. Schematic of the ionogel with salt-adaptive conductivity for submarine sensing. A) The mechanism of improved salt-adaptive conductivity of SDG. B) Schematic diagram of the salt-adaptive sensor working in air and seawater with strengthening signals.

the sensitivity of the ionogel in saline water and weak the impact of the environmental resistor, one of the promising strategies is to increase the ionogel's conductivity, especially in the saline solution, making it predominant in the parallel circuit. Actually, compared to the high conductivity of pure IL, the conductivities of ionogels decrease dramatically because of the introduction of polymer networks which hinder the movement of free ions.[11] Therefore, exploring an ionogel-based sensor with underwater stability and high conductivity is crucial for highly discernible and accurate movement monitoring in aquatic and marine environments, but remains challenging.

Herein, we report an environmental salt-adaptively conductive ionogel (SDG) with high submarine strain sensitivity, which was prepared via facile one-step UV-initiation polymerization. Hydrophobic methyl methacrylate (MMA) was chosen to fabricate a covalently cross-linked skeleton in hydrophobic IL ([BMIm][PF_6]) solvent with great compatibility. To further improve the long-term underwater stability, hydrophobic SiO_2 nanoparticles (NPs) were doped to endow SDG with lower surface free energy while contacting with water. Meanwhile, the proton conductive polymer (PCM) with hydrophilic charged groups (—SO_3^-, —$N(CH_3)_3^+$) was designed for improving the conductivity of SDG, with the hydrophobic part promoting its uniform dispersion in the fully hydrophobic precursor (Figure S1, Supporting Information). As shown in **Figure 1A**, the high salt-adaptive conductivity of SDG is realized by the cooperation between the proton conduction mechanism introduced by PCM and the salt-induced dissociation of IL. First, protons moving along protonic sites (—SO_3H groups) on PCM carry a significant fraction of the current in SDG (Figure 1Ai).[11a] At the same time, in saline solution, the ionogel's conductivity is further activated by the electrostatic attraction of the environmental salt (NaCl), promoting the dissociation of ion pairs at the ionogel surface (Figure 1Aii). Significantly, because of the highly salt-adaptive conductivity, the hydrophobic SDG can act as a flexible sensor in marine environments whose strain-sensing signals are strengthened rather than weakened by the seawater (Figure 1B). The investigation of this kind of environment-adaptive ionogel with intelligent-regulated

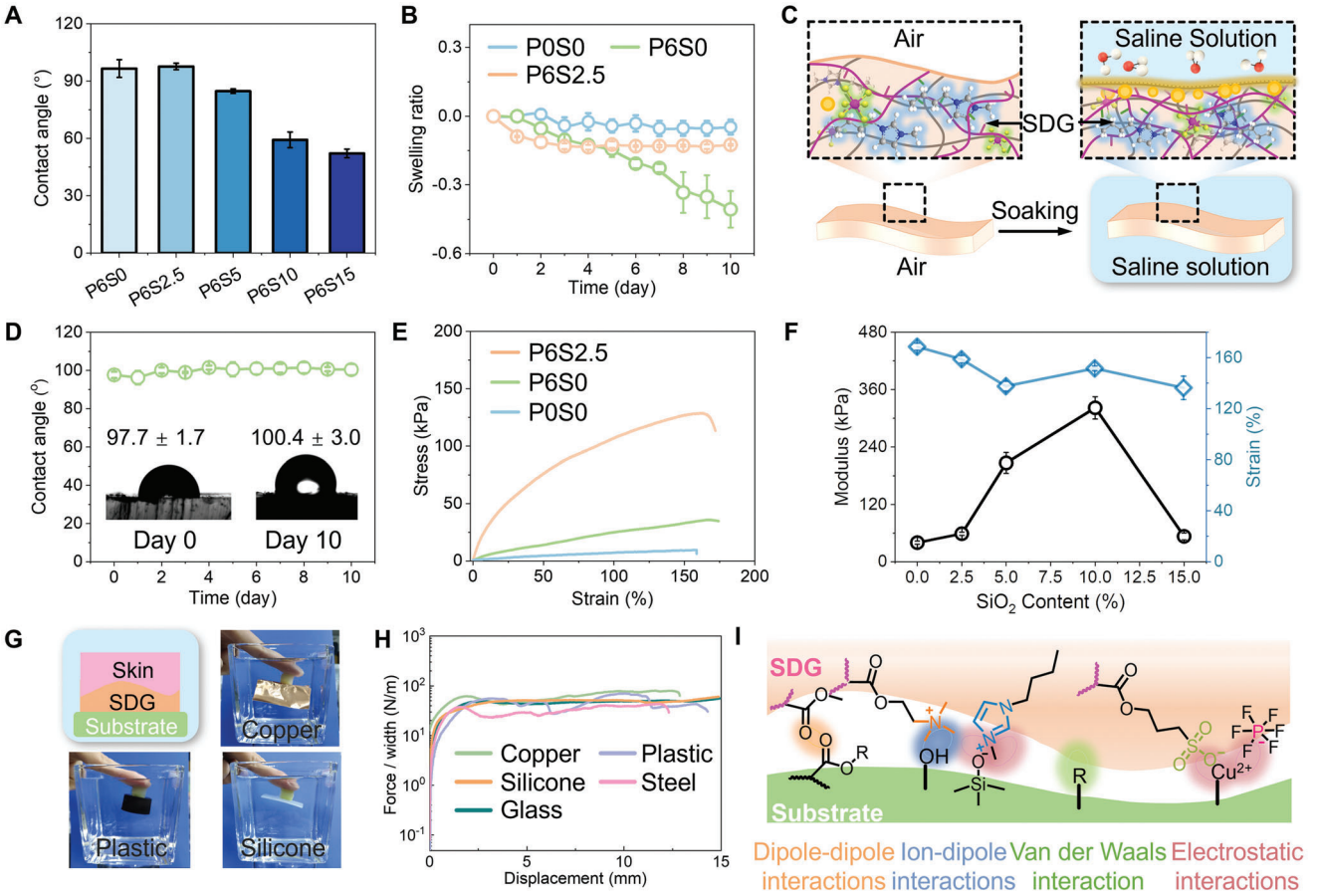

Figure 2. Hydrophobic and mechanical performances of the salt-adaptive ionogel. A) WCA of series ionogels with different PCM and SiO_2 NPs contents. B) Swelling behaviors of ionogels with different PCM and SiO_2 NPs contents. C) Hydrophobic aggregation schematic diagram of polymers and SiO_2 NPs before and after soaking in saline solution. D) WCA change of the ionogel soaking in 3 wt% NaCl solution. E) Tensile curves of the ionogels with different PCM and SiO_2 NPs contents. F) Mechanical properties of the ionogels with different SiO_2 NPs contents. G) Digital images of strong adhesion with various substrates underwater. H) Peeling curves of SDG with various substrates underwater. I) Adhesion mechanisms between SDG and the substrate.

sensing performance is meaningful for ocean exploration without disturbing creatures inside.

2. Results and Discussion

In terms of the underwater long-term stable strain sensor, the hydrophobicity and mechanical properties are the crucial parameters. Here, the PCM content we added changed from 0 to 3, 6, and 9, which were named P0S0, P3S0, P6S0, and P9S0. Since the introduction of hydrophilic parts, the hydrophobicity of the ionogel is weakened, the water contact angle (WCA) dramatically decreasing from 104.8° (P0S0) to 45.1° (P3S0) (Figure S2, Supporting Information). However, the overhigh content of hydrophilic parts forms concentrated polymer clusters but the hydrophobic parts uniformly dominate in the continued IL phase (Figure S3, Supporting Information), causing WCA to recover to 96.1° and 110.0° for P6S0 and P9S0, respectively. Furthermore, with the SiO_2 NPs doping rising from 2.5, 5, 10 to 15 wt%, they were named P*x*S2.5, P*x*S5, P*x*S10, and P*x*S15. After adding SiO_2 NPs, the hydrophobicity of the ionogel becomes stronger, the WCA of P6S2.5 rising up to 97.7° (**Figure 2**A). However, the WCA of P6S15 apparently reduced to 52.1°, which may result from the uneven dispersion of SiO_2 NPs within the ionogel. Furthermore, these ionogels were soaked in 3 wt% NaCl solution to study and imitate their stability in the marine environment. As shown in Figure 2B, compared to the slight weight change of P0S0 (4.8%) in 10 days, although the swelling ratio of P6S2.5 decreased by 11.3% on the second day, there was no significant change over the next 8 days while the weight of P6S0 kept dropping down over 40.7%. The reason why it becomes underwater stable is that, for the fresh ionogel, the distribution of the PMMA network is sparse; after soaking in saline solution, due to its incompatibility with the water surrounding, the network becomes dense and forms a hydrophobic aggregation together with SiO_2 NPs at the surface of ionogel, resulting in lower surface energy (Figure 2C). The lower surface energy can be further confirmed by the change of the WCA, as shown in Figure 2D, the WCA of P6S2.5 evolved from ≈97.7° to ≈100.4° after immersing in 3 wt% NaCl solution for 10 days. Besides, the P6S2.5 exhibited good stability in NaCl solution with different pH values, although the acidity and alkalinity of solution have a slight influence on

the swelling performance of ionogels (Figure S4, Supporting Information).

Meanwhile, the addition of PCM and SiO_2 NPs has a great influence on the mechanical properties of the ionogel. As can be seen from Figure 2E, which was measured by the tensile test, the breaking strain of ionogels increased from 158.0% to 168.5% as the PCM content turned from 0 to 6 wt%. This ascending phenomenon results from the formation of the reversible electrostatic force between the charged side chains which dissipates the energy during stretching (Figure S5, Supporting Information). Moreover, the addition of SiO_2 NPs impacted the mechanical properties. With 2.5 wt% SiO_2 NPs doping (P6S2.5), compared to P6S0, the strain range slightly decreased (158.6%) with the growth of the total solid content. In terms of the mechanical modulus, it increased from 21.5 kPa (P6S0) to 58.6 kPa (P6S2.5) since the reversible hydrophobic interactions formed between NPs and the PMMA network (Figure 2E). However, as shown in Figure 2F, the modulus of the ionogel fell to 53.1 kPa when it came to 15 wt% SiO_2 NPs, after reaching the highest points at 10 wt% content (321.7 kPa). The change of modulus further confirmed the uneven dispersion of excess SiO_2 NPs in ionogel.

The ionogel also presented remarkable underwater adhesive properties. The ionogel can robustly adhere to skin and various substrates in the underwater environment and air, including copper, plastic, silicone, steel, and glass (Figure 2G; Figure S6, Supporting Information). We evaluated the underwater adhesion properties through the 90° peeling-off test (Figure S7, Supporting Information). As shown in Figure 2H, the SDG composite has a peeling force per unit width of 63.54, 59.49, 51.91, 30.83, and 51.34 N m^{-1} with copper, plastic, silicone, steel, and glass substrates underwater on average. Meanwhile, SDG exhibited great long-term adhesion stability in simulated seawater (Figure S8, Supporting Information). The strong adhesion is formed by the noncovalent bonding between polar groups of polymer side chains, IL, and various substrates (Figure 2I), including dipole–dipole interactions, ion–dipole interactions, van der Waals interactions, and electrostatic interactions. Furthermore, these reversible interactions not only bond the ionogel with the substrate toughly when they contact but dissipate energy effectively when they separate. Strong adhesion in air and aquatic environment guarantees accurate sensing during the practical application.

As to the ionogel-based sensor, the essential prerequisite for obtaining high signal intensity in marine is its high conductivity. There are two dominant mechanisms which extremely improve SDG conductivity, as shown in **Figure 3**A. In the air condition, the proposed proton conduction mechanism is depicted in the enlarged circle (Figure 3B). $-SO_3H$ groups introduced by PCM function as proton-active sites. Protons generated from $-SO_3H$ groups associate with $[PF_6]^-$ in IL, hopping and carrying protons from one SO_3^- site to others along the PCM chains. As a validation, a PCM film without IL was prepared. As shown in Figure S9 of the Supporting Information, when the [BMIm][PF_6] was dripped onto the PCM film, there is a distinct potential change in the PCM film due to the IL induced proton dissociation and association. This directional movement of protons carries a significant fraction of the current in SDG. As we can see in Figure 3C, the introduction of PCM in this system enhanced the conductivity of ionogel from 9.18×10^{-2} S m^{-1} (P0S0), which is far lower than the conductivity of pure [BMIm][PF_6] (1.36×10^{-1} S m^{-1}),[12] to 1.85×10^{-1} S m^{-1} (P3S0), and 2.20×10^{-1} S m^{-1} (P6S0). According to the Grotthuss mechanism,[11b] higher PCM content introduced more proton-active sites in the ionogel, namely, more proton transport paths, leading to higher conductivity, which confirmed the existence of proton conduction in SDG. The free ions carried on the PCM function groups also contribute to the increase of conductivity. However, because of the uneven hydrophilic clusters in P9S0 (Figure S3, Supporting Information), the proton-active sites that uniformly disperse in the IL become less, resulting in lower conductivity (1.47×10^{-1} S m^{-1}). The above-descending phenomenon further verified the importance of proton conduction for the improvement of conductivity rather than the free ions from PCM. Meanwhile, the SiO_2 NPs loading would more-or-less hinder the charge transport, reducing the conductivity. The conductivity declined to 9.62×10^{-2} S m^{-1} with 2.5 wt% SiO_2 NPs (P6S2.5), which kept decreasing to 1.20×10^{-2} S m^{-1} for P6S15 (Figure S10, Supporting Information).

It is interesting to note here that soaking in the saline solution would cause significantly higher conductivities than in air conditions, which may be affected by surrounding ions (Figure 3D). P6S2.5 with great conductivity and hydrophobicity was chosen to investigate the conductivity change in various environments. When P6S2.5 was immersed in water, as clearly seen in Figure 3E, the conductivity dropped to 8.43×10^{-2} S m^{-1}, because of the shrinkage of the hydrophobic polymeric network (Figure 2C), impeding the movement of ions. By contrast, the conductivity dramatically rose up to 1.94×10^{-1} S m^{-1} in 1 wt% NaCl solution and kept increasing to 2.90×10^{-1} S m^{-1} in 3 wt% NaCl solution. The conductivity of the SDG in 3.5 wt% sea-salt solution, which is regarded as the simulated seawater, is close to that in 3 wt% NaCl solution, being 2.82×10^{-1} S m^{-1}. Moreover, the conductivity of P6S2.5 was kept at a long-term high level while soaking in the 3 wt% NaCl solution (Figure 3F). Density functional theory is then conducted to gain a better understanding of the mechanism (Equation (S2), Supporting Information). When the ionogel is immersed in the saline solution, there are a large number of free ions moving around it, for instance, Na^+ and Cl^-. As depicted in Figure 3G, the binding energy of $[BMIm]^+$ to Cl^- is the highest, compared to the interaction force between $[BMIm]^+$ and $[PF_6]^-$, Na^+ and $[PF_6]^-$, and Na^+ and Cl^-. The high binding energy indicates that the surrounding Cl^- effectively attracts $[BMIm]^+$ to the surface of ionogel and promotes the dissociation and migration of $[BMIm]^+$ and $[PF_6]^-$, corresponding to higher conductivity. However, when the environmental saline content comes to 3 wt%, the salt-induced dissociation has a saturated tendency, the repulsion between $[BMIm]^+$ may block their further movement toward the surface of SDG. According to the energy-dispersive X-ray spectroscopy analysis, no Na^+ or Cl^- permeates into ionogel before and after soaking for 10 days (Figure S11, Supporting Information), which results from the excellent long-term hydrophobicity of SDG (Figure 2D). Namely, during this period, there is no ion exchange between the saline solution and the ionogel. The phenomena of conductivity varying along with the saline solution were described as the salt-adaptive conductive property, which weakens the influence of environmental resistors and is beneficial for working in the marine environment.

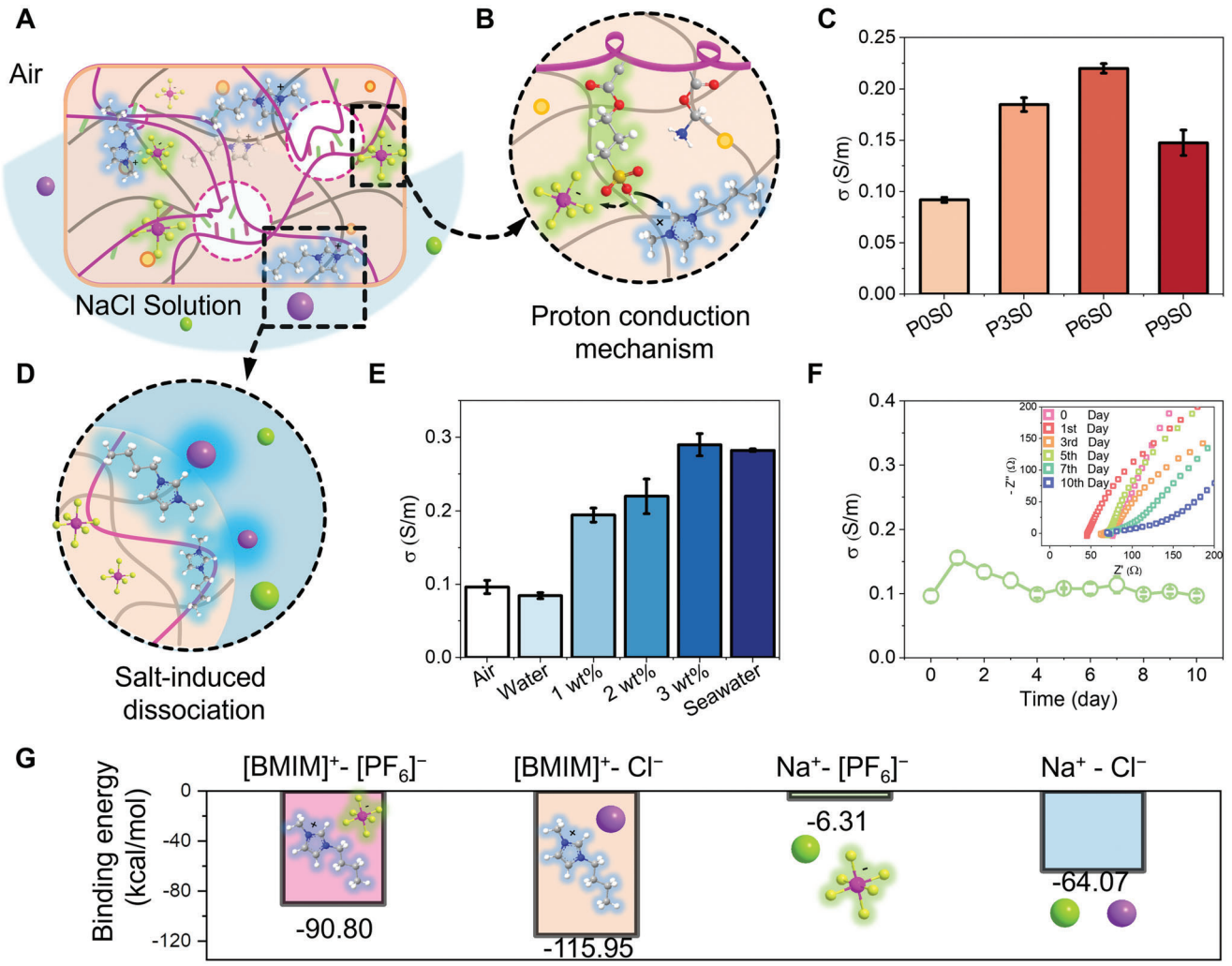

Figure 3. Conductive performance of SDG. A) The schematic illustration of improved salt-adaptive conductivity in SDG. B) The schematic illustration of the proton transport route in the proton conduction mechanism. C) Conductivities of ionogels with different PCM contents in the air. D) Illustration of salt-induced dissociation of SDG in saline solution. E) Conductivity changes of SDG in saline solution. F) The change of SDG conductivity while soaking in 3 wt% NaCl solution. G) The binding energy resulting from density functional theory (DFT) analysis.

Considering the hydrophobic performance, strain range (158.6%), mechanical safety (modulus: 58.6 kPa), and conductivity (9.62×10^{-2} S m^{-1}), P6S2.5 was chosen to be the raw material of the SDG-based sensor. To certify the environmental adaption, the sensing properties of SDG were tested in different environments. The sensing signals are produced under different strains, testing as the normalized electrical resistance change ($\Delta R/R_0$)

$$\Delta R/R_0 = \left(R - R_0\right)/R_0 \quad (1)$$

where R refers to the real-time resistance and R_0 means the initial resistance of SDG at the relaxed state. Meanwhile, the tensile strain (ϵ) was calculated as below

$$\epsilon = \left(L - L_0\right)/L_0 \quad (2)$$

where L and L_0 refer to the SDG length at the tensile state and the relaxed state, respectively. As shown in **Figure 4**A, the relative resistance of SDG showed reversible and stable changes in the low strain range (ϵ: 5–30%), which is close to the degree of body movements and deformation, indicating perfect reliability as the wearable sensor in air condition. Furthermore, to simulate the natural aquatic environment (e.g., salt lakes and oceans), we stretched the sensor in the saline solution with series salinity (1–3 wt%). Interestingly, after being soaked in conductive NaCl solutions, the relative resistance changes became larger and more obvious (Figure 4B; Figure S12, Supporting Information). Specifically, under 30% strain, the value of output signals increased from 15.7% to 23.5%, 33.2%, and 41.2% in air and 1–3 wt% NaCl solution, correspondingly (Figure 4C). Moreover, the gauge factor (GF) was calculated to quantify the sensitivity of SDG, which is defined as the relative ratio of ($\Delta R/R_0$) to tensile strain (ϵ). Compared to the relatively low GF in air condition, being 0.39 (ϵ: 0–50%) and 0.83 (ϵ: 50–100%) (Figure 4D), the GF generally rose up to 1.20 (ϵ: 0–100%) in 3 wt% NaCl solution which we called salt-adaptive sensitivity (Figure S13, Supporting

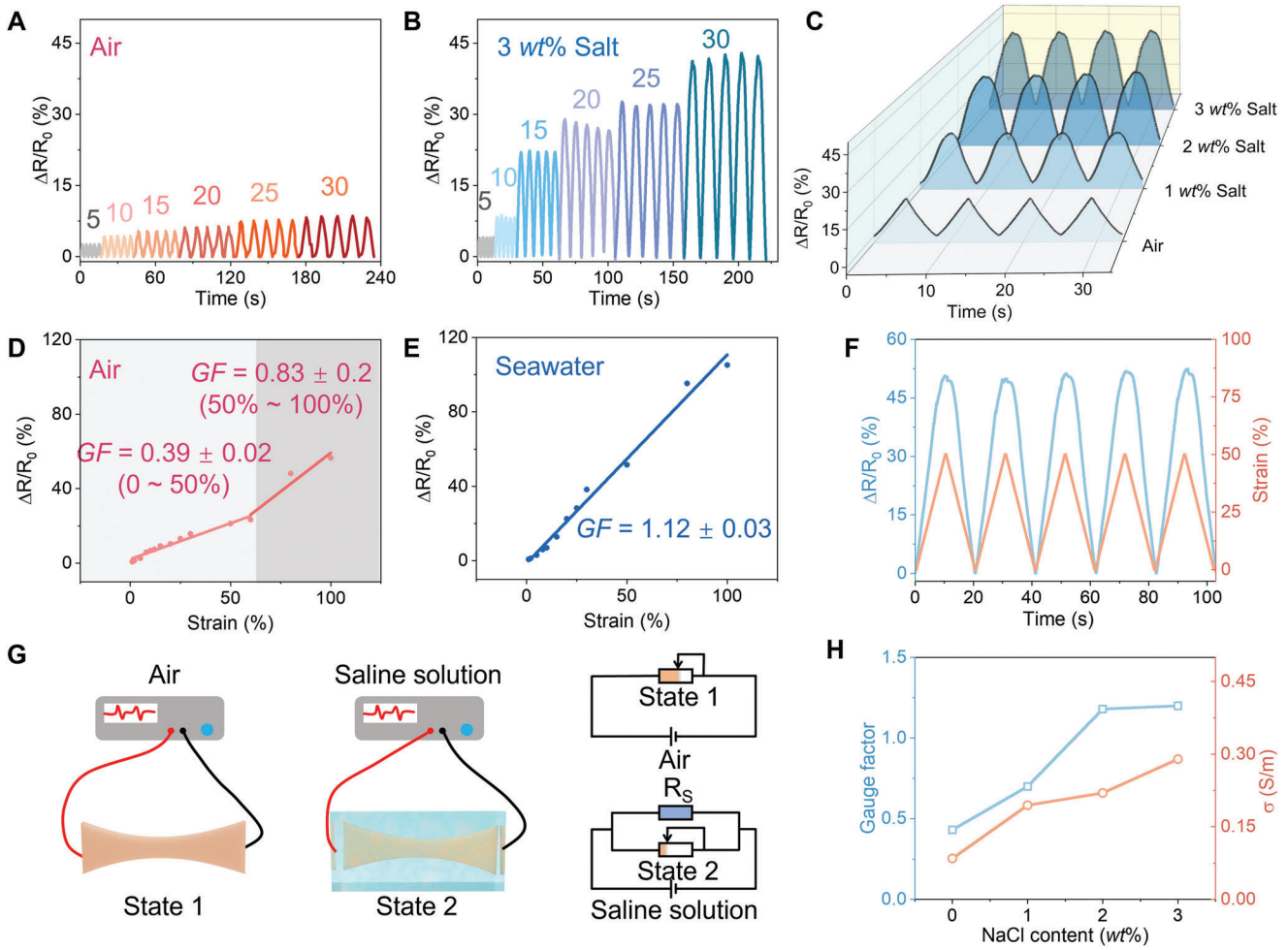

Figure 4. Sensing performance of SDG-based sensor. Relative resistance of SDG-based sensor under series strains in A) air condition and B) 3 wt% NaCl solution. C) The relative resistance comparison of the SDG-based sensor under 30% strain in a series environment. Gauge factor of SDG with segmented strain regions in D) air and E) seawater. F) Tensile strain–time curve and relative resistance–time curve. G) Analog circuit of SDG-based sensor in air and conductive saline solution. H) Relationship between the gauge factor of the SDG-based sensor and its conductivities in series saline solutions.

Information). Benefiting from this property, SDG shows outstanding sensing performance in simulated seawater with GF being 1.12 (ϵ: 0–100%) (Figure 4E). Although this GF value is still not comparable to the sensitivity of high-performance underwater flexible sensors in pure water, it has exceeded the sensing performance of most flexible sensors in seawater environments (Figure S14, Supporting Information).[5b,d,6,10,13] Based on the resistance curve, the response time of SDG in seawater is 3.34 s at 20% strain and the recovery time is 2.88 s (Figure S15, Supporting Information). Meanwhile, there is tiny hysteresis between the relative resistance change and the tensile strain while SDG working in the saline solution, suggesting that the output response signal can keep synchronizing with the input strain changes (Figure 4F). Therefore, it is reliable to achieve the goal of underwater real-time detection with accurate and obvious motion signal output by SDG.

To explain the salt-adaptive sensitivities, we simulated the sensing circuit while the SDG worked in different environments (Figure 4G). In the air condition, there is only one sensor (State 1) connected in the sensing circuit, being responsible for resistance change independently. However, after being soaked in the conductive solution, with the salt-adaptively conductive property, the resistance of SDG drops, turning from State 1 to State 2. At the same time, the environmental resistor (R_s) joined the parallel circuit with the sensor (State 2). According to the simplified derived formula for the GF value in conductive solution (Equation (S5), Supporting Information), the GF value increased with the decreasing $R_{SDG}/R_{Solution}$. Identical conclusions were obtained from the experiment results, the conductivity of SDG rises up rapidly with the salty content increasing (Figure 4H), becoming dominant in the sensing circuit and making the sensing signals more obvious to identify.

On the basis of these results, we concluded that SDG can be used in most natural waters due to its salt-adaptive high conductivity. SDG demonstrated prominent fatigue resistance to strain sensing (Figure S16, Supporting Information). Moreover, SDG presented stable signal outputs even after being soaked in 3 wt% NaCl solution for 3 months (Figure S17, Supporting

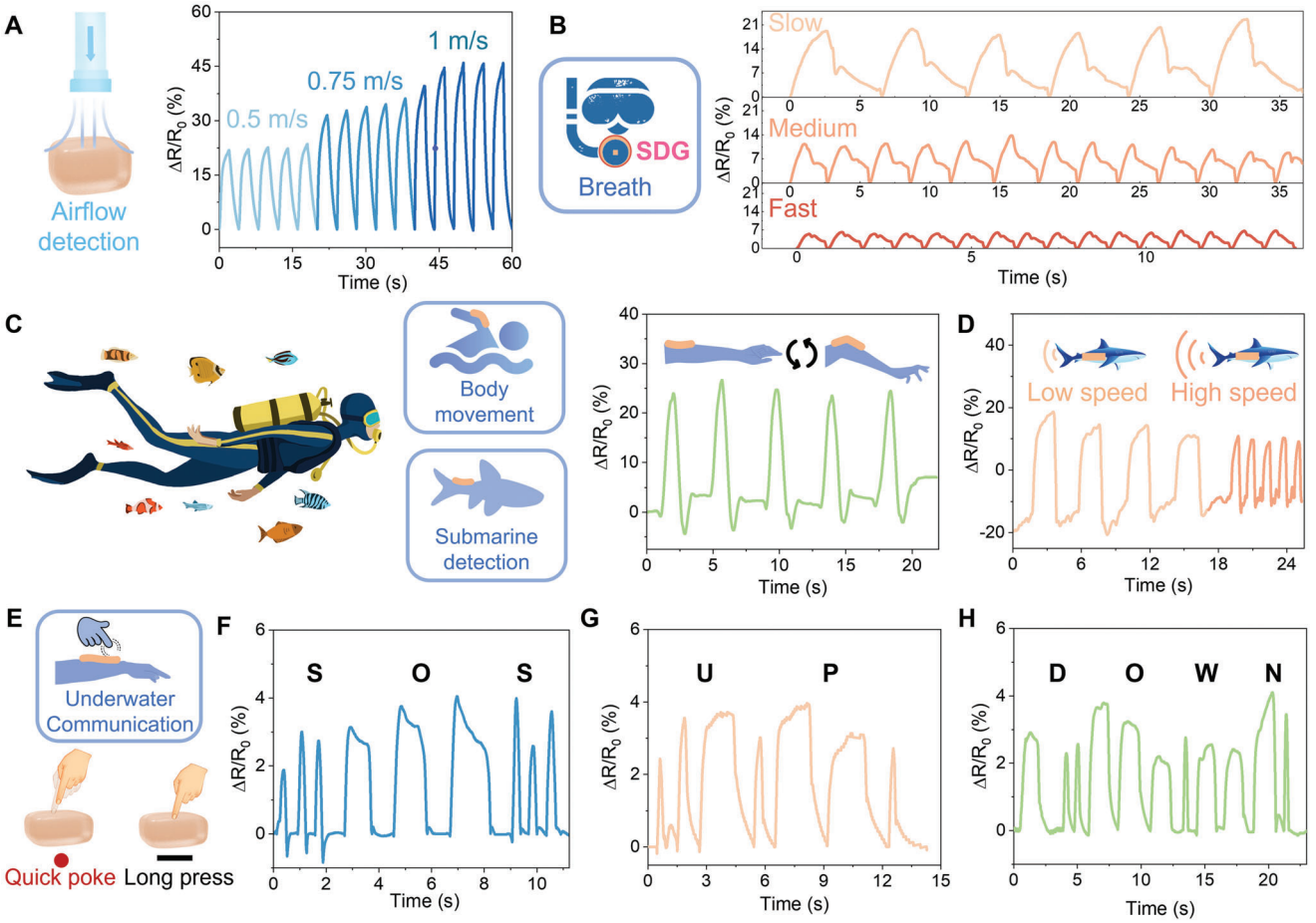

Figure 5. Application of SDG-based sensor for monitoring of breath frequency, human and fish motion, and underwater communication in the marine environment. Relative resistance variation of the SDG-based sensor under different A) airflow rates and B) breath frequency. Schematic diagram and relative resistance variation of the SDG-based sensor for C) human and D) fish robotics body movement detection. Schematic illustration of underwater communication based on E) Morse code, and the resistance signals of F) "SOS", G) "UP", and H) "DOWN".

Information), with slight intensity decay of ≈1.2% (ϵ: 30%) resulting from the unavoidable degradation. The long-term stability benefits from the outstanding hydrophobicity and salt solution adaptive properties of SDG, showing the potential to expand its lifespan in practical applications.

It is well known that diving is one of the crucial ways to explore the marine world. To guarantee the safety of divers during exploration, the change of their life signs should be monitored in real-time, including breath frequency and body movements. However, the conductive seawater would disturb and weaken the sensing process as analyzed before. SDG with merits of hydrophobicity, robust adhesion, and high salt-adaptive sensitivity is promising to be applied as multifunctional sensors in the ocean. Breath frequency is one of the most essential vital signs for a diver. However, the unavoidable seawater penetration in the respiratory mask would interfere with the accuracy of the sensing process. SDG has the ability to sense airflow at different rates due to the formation of subtle deformation on the gel surface caused by gas pressure (**Figure 5**A). As shown in Figure S18 of the Supporting Information, the sensitivity is calculated based on the slope of the relative resistance variation curve, which is 45% m s^{-1} (0–1 m s^{-1}). Based on the desired performance of the SDG-based sensor, we demonstrate its potential application as a breathing monitor, excluding the influence of seawater penetration during diving. The SDG-based sensor adhered to the respiratory mask records the breath process during simulated swimming. The frequency of breath was accurately perceived and differentiated (Figure 5B), suggesting that the exercise intensity and oxygen consumption of the diver can be roughly evaluated in time. Furthermore, since the opaque feature of marine, it is unreliable to tell the working statement of divers and soft actuators via visual observation. However, recognizing their movements in real time is an essential precondition for the protection of divers and precise control of soft actuators. Owing to its fascinating high strain sensitivity in saline solution, the multifunctional SDG-based sensor can be fixed on the surface of the skin or other soft actuators directly for locomotion detection (Figure 5C). For example, when it was stuck to the elbow, the state of breaststroke can be distinguished clearly. The motion of marine organisms in most natural waters can also be detected by attaching SDG to their bodies. As a demonstration, the swimming state of the shark model was detected by fixing the sensor on its tail (Figure 5D). By analyzing the intensity and frequency of the signals, the swimming speed of the shark model can be estimated. Moreover, efficient and accurate

underwater communication, which helps the diver send urgent messages about rescue actions, is expected to reduce the probability of accidents. For this, the pressure-sensing ability of the freestanding SDG-based sensor can be used for the underwater communicator with Morse code (Figure S19, Supporting Information). For this communicator, the quick poke means dots in the Morse code while the long press means dashes (Figure 5E). Therefore, a series of necessary messages can be shared between divers easily. For example, "SOS" can be sent out for help (Figure 5F), the words "up" (Figure 5G), "down" (Figure 5H), right (Figure S20A, Supporting Information), and left (Figure S20B, Supporting Information) for changing the diving directions. Figure S21 of the Supporting Information schematically demonstrates the application of the SDG-based sensor in soft gripper sensing. When it is gripping an object in seawater, the bending motion of the soft gripper finger can be detected by sticking the SDG sensor on the outer surface. During the gripper carrying the gripping task, for instance, with objects of a larger volume, the more obvious bending motion happens on the soft fingers and the more apparent resultant signals ($\Delta R/R_0$) outputs. Therefore, according to the signals, not only the locomoting state of soft actuators can be monitored, but the information of objects, which are caught can be acquired. The above demonstrations extremely show the great potential of SDG-based sensors in monitoring the movements of marine organisms and robotics, which can be further applied for the construction of perceptive soft robotics and surveillance equipment in the marine environment.

3. Conclusion

In summary, an environmental salt-adaptively conductive ionogel with high submarine strain sensitivity has been fabricated via a simple one-step polymerization. To improve the sensing performance of the ionogel in the marine environment, the conductivity of the ionogel was increased by the cooperation of the proton conduction mechanism with salt-induced dissociation. The proton conduction enhanced the ion transport rate by creating a shortcut for proton transport along the PCM polymer chains with $-SO_3H$ groups. Meanwhile, by virtue of the strong appealing force between the cations inside the ionogel ($[BMIm]^+$) and Cl^- from the surrounding saline solution, the dissociation of ion pairs in ionogel rises up, increasing the number of free ions, resulting in salt-adaptive conductivity improvement. The conductivities of obtained ionogel in saline water are orders of magnitude higher than those without PCM chains. More significantly, the high conductivity makes the ionogel dominate the sensing circuit while working in seawater. Specifically, owing to the great hydrophobic and adhesion properties of the ionogel, it realized accurate strain-sensing of various soft actuators in marine environments, including marine organisms and soft robotics. At the same time, the freestanding ionogel-based sensor can serve as the breathing monitor, underwater communicator for divers' safety. These results are expected to provide promising strategies for developing highly sensitive, multimodal sensing ionogel, which can be used to design flexible sensors and perceptive intelligent soft actuators in low visible marine environments.

Supporting Information

Supporting Information is available from the Wiley Online Library or from the author.

Acknowledgements

This work was supported by the National Natural Science Foundation of China (52103152), China Postdoctoral Science Foundation (2021M690157 and 2022T150668), Ningbo Key R&D Program (2023Z089), and Ningbo Natural Science Foundation (2121J206).

Conflict of Interest

The authors declare no conflict of interest.

Data Availability Statement

The data that support the findings of this study are available from the corresponding author upon reasonable request.

Keywords

high strain sensitivity, hydrophobic ionogel, marine exploration, salt-adaptive conductivity

Received: July 30, 2023
Revised: August 22, 2023
Published online:

[1] a) R. K. Katzschmann, J. DelPreto, R. MacCurdy, D. Rus, *Sci. Robot.* **2018**, *3*, 3449; b) D. R. Yoerger, A. F. Govindarajan, J. C. Howland, J. K. Llopiz, P. H. Wiebe, M. Curran, J. Fujii, D. Gomez-Ibanez, K. Katija, B. H. Robison, B. W. Hobson, M. Risi, S. M. Rock, *Sci. Robot.* **2021**, *6*, 1901; c) R. A. Lutz, P. G. Falkowski, *Science* **2012**, *336*, 301.

[2] K. Liu, Y. Jiang, Z. Bao, X. Yan, *CCS Chem.* **2019**, *1*, 431.

[3] a) H. Li, G. Gao, Z. Xu, D. Tang, T. Chen, *Macromol. Rapid Commun.* **2021**, *42*, 2100480; b) D. Zhang, B. Ren, Y. Zhang, L. Xu, Q. Huang, Y. He, X. Li, J. Wu, J. Yang, Q. Chen, Y. Chang, J. Zheng, *J. Mater. Chem. B* **2020**, *8*, 3171; c) Y. Niu, H. Liu, R. He, Z. Li, H. Ren, B. Gao, H. Guo, G. M. Genin, F. Xu, *Mater. Today* **2020**, *41*, 219.

[4] G. Li, C. Li, G. Li, D. Yu, Z. Song, H. Wang, X. Liu, H. Liu, W. Liu, *Small* **2022**, *18*, 2101518.

[5] a) J. Wei, P. Xiao, T. Chen, *Adv. Mater.* **2023**, *44*, 2211758; b) Z. Wang, H. Zhou, D. Liu, X. Chen, D. Wang, S. Dai, F. Chen, B. B. Xu, *Adv. Funct. Mater.* **2022**, *32*, 2201396; c) T. Chen, P. Wei, G. Chen, H. Liu, I. T. Mugaanire, K. Hou, M. Zhu, *J. Mater. Chem. A* **2021**, *9*, 12265; d) J. Ren, Y. Liu, Z. Wang, S. Chen, Y. Ma, H. Wei, S. Lü, *Adv. Funct. Mater.* **2021**, *32*, 2107404.

[6] L. Ma, J. Wang, J. He, Y. Yao, X. Zhu, L. Peng, J. Yang, X. Liu, M. Qu, *J. Mater. Chem. A* **2021**, *9*, 26949.

[7] a) J. Y. Sun, C. Keplinger, G. M. Whitesides, Z. Suo, *Adv. Mater.* **2014**, *26*, 7608; b) D. Zhang, M. Zhang, J. Wang, H. Sun, H. Liu, L. Mi, C. Liu, C. Shen, *Adv. Compos. Hybrid Mater.* **2022**, *5*, 1812; c) Y. Zhang, W. Zhang, G. Ye, Q. Tan, Y. Zhao, J. Qiu, S. Qi, X. Du, T. Chen, N. Liu, *Adv. Mater. Technol.* **2019**, *5*, 1900880; d) G. Ge, Y. Lu, X. Qu, W. Zhao, Y. Ren, W. Wang, Q. Wang, W. Huang, X. Dong, *ACS Nano* **2020**, *14*, 218.

[8] a) L. Shi, K. Jia, Y. Gao, H. Yang, Y. Ma, S. Lu, G. Gao, H. Bu, T. Lu, S. Ding, *Research* **2020**, *2020*, 2505619; b) A. Hu, C. Liu, Z. Cui, Z. Cong, J. Niu, *ACS Appl. Mater. Interfaces* **2022**, *14*, 12713; c) Y. Cao, Y. J. Tan, S. Li, W. W. Lee, H. Guo, Y. Cai, C. Wang, B. C. K. Tee, *Nat. Electron.* **2019**, *2*, 75; d) Z. Lei, P. Wu, *Nat. Commun.* **2019**, *10*, 3429; e) X. Wan, Y. He, Z. Xu, C. Li, C. Yang, *Macromol. Rapid Commun.* **2023**, *44*, 2200957.
[9] Z. Yu, P. Wu, *Adv. Mater.* **2021**, *33*, 2008479.
[10] J. Wei, Y. Zheng, T. Chen, *Mater. Horiz.* **2021**, *8*, 2761.
[11] a) S. Y. Kim, S. Kim, M. J. Park, *Nat. Commun.* **2010**, *1*, 88; b) E. Cho, J.-S. Park, S. S. Sekhon, G.-G. Park, T.-H. Yang, W.-Y. Lee, C.-S. Kim, S.-B. Park, *J. Electrochem. Soc.* **2009**, *156*, B197.
[12] H. Cheng, Q. Le, Z. Liu, Q. Qian, Y. Zhao, J. Ouyang, *J. Mater. Chem. C* **2022**, *10*, 433.
[13] a) Z. Zhang, G. Chen, Y. Xue, Q. Duan, X. Liang, T. Lin, Z. Wu, Y. Tan, Q. Zhao, W. Zheng, L. Wang, F. Wang, X. Luo, J. Xu, J. Liu, B. Lu, *Adv. Funct. Mater.* **2023**, *44*, 2305705; b) M. Pi, S. Qin, S. Wen, Z. Wang, X. Wang, M. Li, H. Lu, Q. Meng, W. Cui, R. Ran, *Adv. Funct. Mater.* **2022**, *33*, 2210188; c) Z. Wang, D. Wang, D. Liu, X. Han, X. Liu, H. Torun, Z. Guo, S. Duan, X. He, X. Zhang, B. B. Xu, F. Chen, *Adv. Funct. Mater.* **2023**, *33*, 2301117.